MTLA 30 (2023) 101819

Contents lists available at ScienceDirect

Materialia

journal homepage: www.elsevier.com/locate/mtla

Full length article

# Effect of stacking order in cylindrical geometry on the growth of $ZnAl_2O_4$ spinel phase

Gergő Vecsei [a,b], Gabriella Jáger [a,b], Laura Juhász [a], János J. Tomán [a], Vincent Otieno Odhiambo [c], Imre Miklós Szilágyi [c], Zoltán Erdélyi [a], Csaba Cserháti [a,*]

[a] Department of Solid State Physics, Faculty of Science and Technology, University of Debrecen, P.O. Box. 400, Debrecen, H-4002, Hungary
[b] Department of Solid State Physics, Doctoral School of Physics, Faculty of Science and Technology, University of Debrecen, P.O. Box. 400, Debrecen, H-4002, Hungary
[c] Department of Inorganic and Analytical Chemistry, Budapest University of Technology and Economics, Szt. Gellért sqr. 4, Budapest, H-1111, Hungary

ARTICLE INFO

*Keywords:*
Interface diffusion
Stress assisted diffusion
Kinetics
Spinel
Scanning/transmission electron microscopy

ABSTRACT

Growth kinetics of $ZnAl_2O_4$ spinel phase was followed in double layered nanotubes (DLNTs), i.e. in cylindrical geometry in two different layer sequences. DLNTs were annealed at 700 °C in ambient atmosphere for different times. $ZnAl_2O_4$ phase formed due to solid-state reaction. To follow the growth kinetics of the spinel, thin lamellae were prepared from the cross sections of the tubes and studied in a transmission mode scanning electron microscope (TSEM). The phase grows parabolically with time, independently of the layer sequence. The growth rate was higher in the )ZnO)$Al_2O_3$) layer sequence, than for the reverse case. This can be explained by the competing vacancy fluxes induced by mechanical stress developing during the solid-state reaction and by the difference in the diffusion fluxes of the two constituents. This is the first case that the influence of closed geometry and layer sequence on spinel growth between two oxide layers has been experimentally investigated.

## 1. Introduction

Kirkendall effect is a well-known phenomenon during interdiffusion in binary systems [1]. The origin of this effect is the resultant vacancy flow caused by the inequality of the intrinsic atomic fluxes in the lattice frame of reference oriented towards the faster component. In fact this resultant volume flow is responsible for the development of stress in the diffusion zone: one side tends to shrink and the other one to expand. Additional stress can also develop due to the formation of product compounds in which the specific volumes of the constituents can be considerably different than in the parent phases [2]. The developed stress field may in turn have a feedback effect on the atomic fluxes. Since the stress fields are long-range fields, for samples with closed geometries, e.g. cylindrical or spherical samples, the stress development and relaxation will certainly depend on the shape and size of the sample and for example the dependence of the process on the radius and the stacking sequence is expected [2,3]. Even nowadays, describing the complex interplay of diffusion and stress is a challenge.

The effect of closed geometry and diameter variation on the growth of intermetallic layers has been investigated for a while in macroscopic samples. One of the first experimental findings dates back to 1977 when they demonstrated that in a Ni-Cd system with a closed geometry, the formation of the $Ni_5Cd_{21}$ phase led to cracks and local separation of layers, while this effect in planar geometry was not observed [4,5]. In 1990, a detailed investigation regarding phase growth in the cylindrical Cu-Zn system was performed by Bogdanov et al. [6]. Our research group also investigated the growth of $\Theta$ (Al Cu), $\eta_2$ (AlCu) and $\delta$ ($Al_2Cu_3$) phases in the Al-Cu system (Al wire covered by copper), as well as the growth of $\gamma$ ($Ni_5Cd_{21}$) and $\gamma'$ ($Cd_2Ni$) phases in Cd-Ni system in planar and cylindrical geometry at different radiuses and temperatures [7,8].

In 2012 and 2017, theoretical descriptions of reactive diffusion in spherical and cylindrical core–shell nanostructures were developed by Erdélyi et al. [9] and Roussel et al. [10].

To demonstrate the interplay between stress and solid-state reaction, Schmitz et al. [3] designed a clear model experiment by depositing thin-film Al/Cu/Al and Cu/Al/Cu triple layers on tips of 25 nm apex radius and investigated them by atom probe tomography (APT). They studied the growth of the reaction product, which was always faster when the Cu was stacked on top of Al. They suggested, that an analogous effect may play a role in oxidation or chemical reactions of core–shell structures.

The study of how solid-state reactions take place in closed geometries is also relevant for applications. Double- or multilayer nanotubes

* Corresponding author.
*E-mail address:* cserhati.csaba@science.unideb.hu (C. Cserháti).

https://doi.org/10.1016/j.mtla.2023.101819
Received 2 November 2022; Accepted 8 June 2023
Available online 9 June 2023

are promising materials in the production of gas sensors, chemical and biochemical sensors and solar cells. In most cases, the formation of these structures is based on solid-state diffusion and/or reaction between two parent materials, and the Kirkendall effect is applied to explain the resulting arrangements [11–14]. Choosing the appropriate constituents, solid-state reactions can result in spinel nanostructures, which are of great interest due to their wide range of applicability [15–18]. Specifically, zinc-aluminate has been chosen because $ZnAl_2O_4$ is the only phase that exists in the equilibrium $ZnO/Al_2O_3$ phase diagram [19] and there is a number of technological applications in which $ZnAl_2O_4$ is a promising candidate. As a catalyst [20] or photocatalytic material, it is particularly suitable for the elimination of toxic aromatic compounds [21] but it also shows potential as a temperature sensor [22] and its good thermal stability makes it suitable for high temperature applications [15,23].

In the present work, the main aspect of the investigation was to study the kinetics of the $ZnAl_2O_4$ spinel growth in different stacking orders of ALD-grown ZnO and $Al_2O_3$ oxide layers in double-layered nanotubes (DLNTs), i.e. cylindrical geometry. $ZnAl_2O_4$ forms in the solid state reaction (SSR) $ZnO + Al_2O_3 \rightarrow ZnAl_2O_4$, where Zn and Al are metallic elements with valencies $2^+$ and $3^+$ respectively and O with a valency of $2^-$. Because of the many various application possibilities listed above, understanding the underlying processes of spinel formation and growth are indispensable. This work presents experimental results that can help us gain a deeper understanding of the interplay between reactive diffusion and stress and initiate further experimental studies on this subject.

## 2. Experimental

Poly(vinyl alcohol) (PVA) nanofibers, prepared via electrospinning method [24], were used as templates (core) to produce nanowires in two sequences, PVA)$Al_2O_3$)ZnO) and PVA)ZnO)$Al_2O_3$), by atomic layer deposition (ALD) in a Beneq TFS-200 – 186 reactor. $Al_2O_3$ layer was prepared using trimethylaluminium (TMA) and water ($H_2O$) as precursors at 70 °C. The pulse time for the TMA and $H_2O$ was 0.15 s [25] which was followed by a 6 s and 10 s nitrogen purge. For the ZnO layer diethyl-zinc (DEZ) and water ($H_2O$) precursors were used at 100 °C. The consecutive pulse times were: 0.15 s for DEZ followed by a 10 s nitrogen purge and 0.15 s for $H_2O$ followed by 10 s nitrogen purge [26]. 240 cycles of $Al_2O_3$ and 100 cycles of ZnO have been deposited on glass samples to determine the deposition rate of the metal oxides. X-ray reflectivity (Rigaku SmartLab 9 kW X-ray diffractrometer), variable angle spectroscopic ellipsometry (Semilab SE-2000) as well as profilometer (AMBIOS XP-I.) measurements were performed to determine the deposition rates of the different oxide layers which were found to be 0.07 nm/cyc for $Al_2O_3$ and 0.1 nm/cyc for ZnO. After deposition, the samples were annealed in ambient atmosphere in order to eliminate the PVA core, resulting in DLNTs in two different stacking orders:)$Al_2O_3$)ZnO) and)ZnO)$Al_2O_3$). The heat treatments were carried out in tube furnace using the following program [24]: (1) the temperature was increased from room temperature up to 230 °C with 10 °C/min heating rate, then (2) it was further increased up to 550 °C with 2 °C/min heating rate. After reaching 550 °C, the samples were removed from the furnace and cooled down to room temperature.

To initiate the spinel formation, the pre-treatment step was followed by further annealing of DLNTs in ambient atmosphere for different periods of time at 700 °C in the same tube-furnace.

In every stage of the experimental process, X-ray diffraction patterns were collected using the X-ray diffractometer (XRD) under Cu-$K_\alpha$ radiation (1.54 Å) in order to detect and identify the appearing $ZnAl_2O_4$ phase. Cross-sectional TEM (X-TEM) lamellae were prepared from the samples using Thermo Fisher Scientific Scios 2 dual beam scanning electron microscope (FIB-SEM), and images were taken at 30 kV in the FIB-SEM using a retractable STEM detector in transmission mode (TSEM). SEM, as well as TSEM images, were used to measure the initial thicknesses of the as-deposited layers as well as the thickness of the $ZnAl_2O_4$ spinel formed during the reaction–diffusion process. It is important to emphasize that during the measurements we focused on the growth aspect of the reaction–diffusion process.

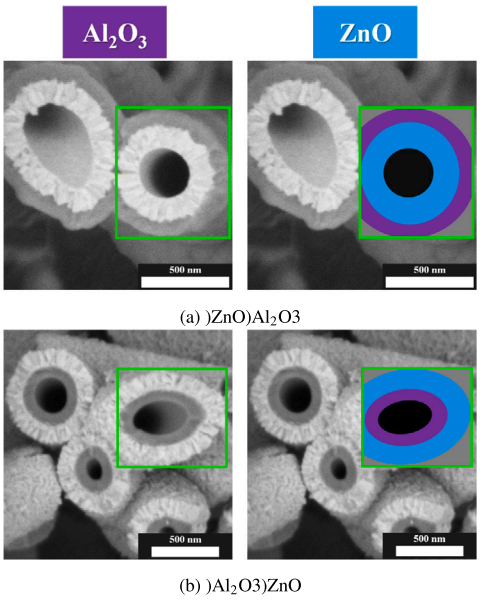


**Fig. 1.** Z-contrast (BSE) images of the two types of nanotubes after the preannealing step. For better interpretation, see the schematics on the right. The images were taken at 2 kV using the in-lens BSE detector.

## 3. Results

Fig. 1 displays both sample sequences after the PVA template was burned out during the pre-treatment. The images were taken from the fractured end of the DLNTs in Z-contrast mode. The average thicknesses of the deposited layers determined via TSEM image analysis are ~150 nm and ~75 nm for the ZnO and the $Al_2O_3$ respectively.

X-TEM lamellae were prepared and XRD diffractograms were taken after each heat treatment step. The measured X-ray diffractograms taken from the as-deposited samples showed peaks of the ZnO phase, indicating that only the ZnO layer was crystalline, while the $Al_2O_3$ was amorphous (see Fig. 3). The TSEM measurements on the heat treated samples showed that while in one stacking order the zinc-aluminate phase can appear after only one hour of annealing at 700 °C, it takes longer in the reverse order. Note, that our earlier measurements [27] on the formation of the $ZnAl_2O_4$ in planar geometry showed that the new intermediate phase appears after 15 min of annealing at the same temperature.

Fig. 2 displays TSEM images of the DLNTs annealed at 700°C for 640 minutes with both stacking order.

It is known that the formation of pores during interdiffusion is a consequence of the resulting vacancy flow, $J_v$, which is oriented against the faster diffusing component. Although details of the nucleation and growth of the void(s) can be complicated due to additional effects, such as stress development [28–30], non-steady-state vacancy distribution [31] etc., it is generally accepted that the overall growth of the voids is controlled by the faster diffusing component.

In Fig. 2 Frenkel-voids are visible at the ZnO side of the new $ZnAl_2O_4$ phase in both layer sequences. This indicates that ZnO is the faster (often supposed as the only) moving component in the system, which is in agreement with earlier investigations [12,32,33]. The process is understood in terms of a uni-directional vacancy diffusion mechanism, wherein ZnO diffuses into the $Al_2O_3$ layer, resulting in vacancy accumulation and supersaturation at the ZnO side of the spinel

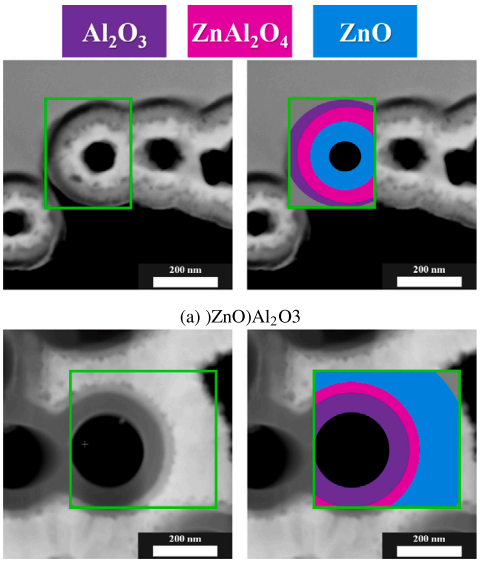


(a) )ZnO)$Al_2O3$

(b) )$Al_2O3$)ZnO

**Fig. 2.** TSEM images of the two types of nanotubes annealed at 700°C for 640 minutes. The images were taken at 30 kV in TSEM-HAADF mode, it shows Z-contrast. For better interpretation, see the coloured details on the right. (For interpretation of the references to colour in this figure legend, the reader is referred to the web version of this article.)

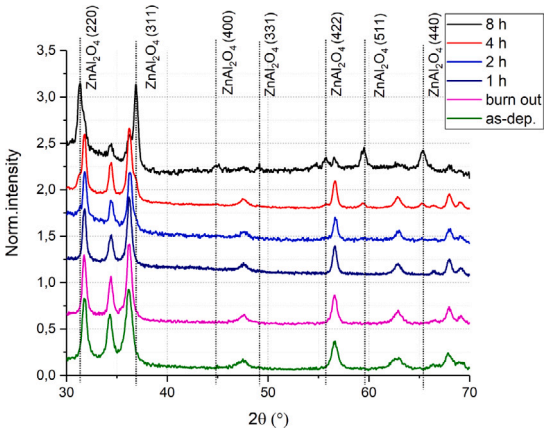


**Fig. 3.** X-ray diffractograms of )ZnO)$Al_2O_3$) specimens after different annealing times. Black vertical lines and indices correspond to spinel ($ZnAl_2O_4$) Bragg peaks. The unindexed peaks show the diffraction pattern of the ZnO phase. After 2 h of heat treatment, the appearing shoulders of ZnO at values of 31.78° and 36.8° confirm the appearance of $ZnAl_2O_4$. After 8 h of heat treatment, the peaks of the spinel phase became more significant, on the other hand, we could observe a slight decrease in the ZnO peaks.

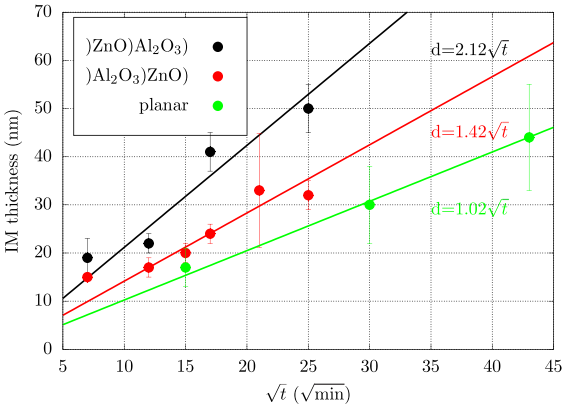


**Fig. 4.** Layer thickness of the $Al_2ZnO_4$ intermediate phase as a function of the square root of the annealing time. The points show the corresponding experimental data of the different layer sequences in cylindrical geometry for )ZnO)$Al_2O_3$) (black) and for )$Al_2O_3$)ZnO) (red) type samples. Note, that the thicknesses of the continuous layers are plotted, i.e. we focused on the growth phase of the whole process. The green points display data of the planar sample [27]. (For interpretation of the references to colour in this figure legend, the reader is referred to the web version of this article.)

phase. Voiding is a result of the relaxation of the material supersaturated with vacancies. The relaxation of the vacancy subsystem in ionic materials can proceed in this way, which means just joining vacancies into voids [34–36]. It cannot be directly determined if the reaction proceeds via molecular or cation-anion movement, but the appearance of the voids indicate which is the faster diffusing component [33].

Another interesting experimental finding is, that a continuous new phase appears earlier in the )ZnO)$Al_2O_3$) type samples, then in the reverse order. In the case of the )ZnO)$Al_2O_3$) type of specimen the initial interface was wavy, due to the polycrystallinity of the ZnO. The grain size, as in most thin films, is comparable to the layer thickness of the ZnO film. In the case of the other sequence, the originally sharp $Al_2O_3$/ZnO interface resulted in a more even growth of the $ZnAl_2O_4$ phase, which nucleates and forms a continuous layer a bit later (see Fig. 4).

X-ray diffractograms (Fig. 3) taken from the specimens show the appearance of the $ZnAl_2O_4$ phase. Comparing the peak heights of the different phases in the diffraction spectra of samples heat-treated for different times indicate the growth of the spinel and the consumption of the zincite, since the height of the $ZnAl_2O_4$ peaks increase, while that of the ZnO peaks decrease.

In Fig. 4 the layer thicknesses of the $ZnAl_2O_4$ phase are plotted as a function of the square root of the annealing time for both layer sequences. One can see, that the experimental points in both cases can be well fitted with straight lines, indicating that the growth follows parabolic kinetics in both cases, i.e. $\Delta x = \Delta P\sqrt{t}$, where $\Delta x$ is the layer thickness of the new phase, $\Delta P$ is the growth rate constant, which is generally temperature dependent and $t$ is the annealing time [1]. The plot displays that, according to the fitting, the growth is faster, i.e. $\Delta P$ is greater in the )ZnO)$Al_2O_3$) type DLNT than in the other sequence.

## 4. Discussion and conclusion

In conclusion, we showed that between crystalline ZnO and amorphous $Al_2O_3$ a crystalline $ZnAl_2O_4$ spinel phase forms at 700 °C in cylindrical geometry. The reaction product grows into the alumina phase, producing Frenkel-voids at the ZnO/$ZnAl_2O_4$ interface independently of the layer sequence. This is a clear indication that the solid-state reaction process is controlled by ZnO diffusion. It also appeared, that the spinel layer starts to grow earlier in the )ZnO)$Al_2O_3$), than for the )$Al_2O_3$)ZnO) arrangement. We found that the growth kinetics follows a parabolic time dependence independently of the stacking. The growth rate is higher for the )ZnO)$Al_2O_3$) type of sample than for the )$Al_2O_3$)ZnO) one.

Since the specific volume of the product phase is greater than the specific volume of the mother phases, in cylindrical geometry, the developing mechanical stress field is such that there is tensile stress in the outer and compressive stress in the inner side of the product phase, which induces a vacancy flux towards the inside of the nanotube (stress field induced vacancy flux) [3,9,10]. Moreover, this is independent of the initial stacking order of the oxides (see Fig. 5).

On the other hand, because of the difference of the diffusion fluxes of the components, there is always a resulting vacancy flux towards the faster component (it is induced by the imbalance of the atomic fluxes) [1] (see Fig. 5).

As a result, if the faster component is in the inner layer, then the vacancy fluxes induced by the stress field and the imbalance of

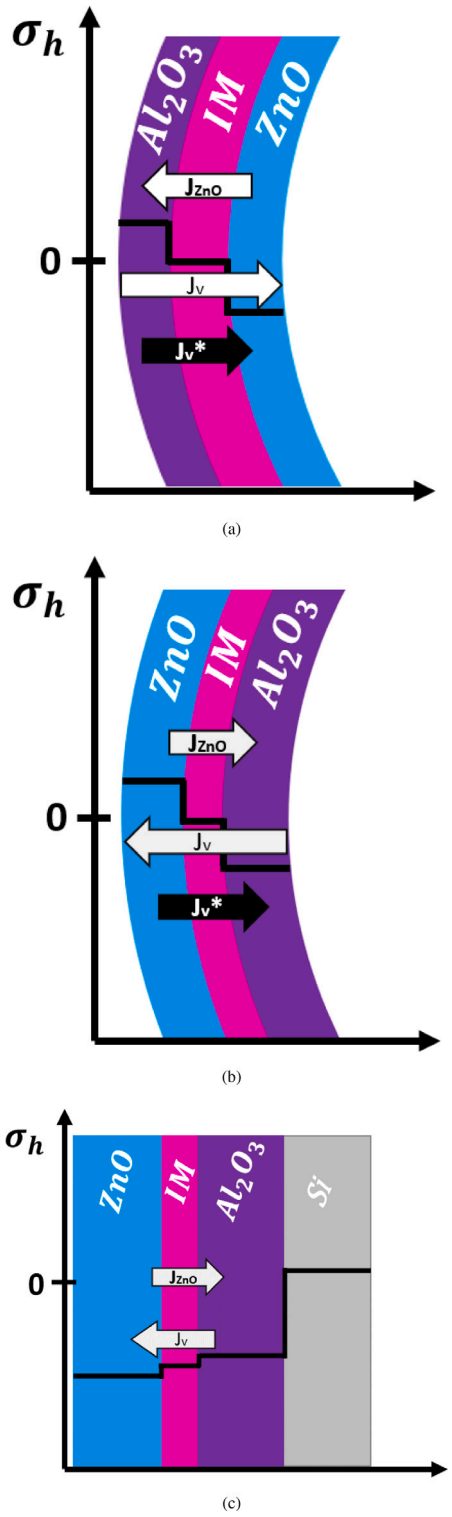


**Fig. 5.** Schematic figure of the developing hydrostatical stress (black curve), the atomic ($J_{ZnO}$, grey arrow) and vacancy fluxes ($J_v$ and $J_v*$) in different layer sequences. The black ($J_v*$) arrow shows the mechanical stress induced vacancy flux, whereas the grey ($J_v$) arrow displays the vacancy flux due to the imbalance of the atomic fluxes. (on the basis of [9,10]).

the atomic fluxes are parallel, which helps the diffusion of the ZnO, resulting faster growth of the spinel product, whereas if the slower component is the inner layer, they are antiparallel, so the phase growth is slower (see Fig. 5).

There are theoretical and experimental evidences [37] which support that positive nanoscale curvature i.e. concave surface is able to considerably increase the probability of phase nucleation and even contributes considerably to the growth rate of the nuclei. This explains that the continuous new phase appears earlier in the )ZnO)$Al_2O_3$) type samples, than in the reverse case. It is important, that the phase growth in this cylindrical case follows a parabolic time dependence (see Fig. 4). The reason of this could be, that grain coarsening is not as easy in this geometry, than in planar one, i.e. only the grain boundary diffusion of the ZnO (either in ionic or in molecular form) controls the growth of the new $ZnAl_2O_4$ phase [38].

Comparing the growth rate of the spinel in planar [27] and cylindrical geometry, one can immediately see that it is the slowest in planar case (see Fig. 4). This may be surprising, since based on our previous calculations [9,10], we would expect this to fall between the two growth rates measured in the cylindrical samples. The discrepancy can be explained by the fact that stress field develops not only due to material transport, but also due to thermal expansion. The planar samples were produced on a rigid Si substrate, i.e. its presence greatly influences the process through the different thermal expansion of the substrate and the sample. According to the available data, the thermal expansion coefficient for Si is $\sim 10^{-6}$1/K, while for ZnO and $Al_2O_3$ it is practically the same and one order of magnitude higher ($\sim 10^{-5}$1/K) than that of the substrate.

The developing thermal stress, even in multilayered samples, can be calculated using the following formula [39,40]:

$$\sigma(z) = \frac{E(z)}{1-\nu(z)}[\varepsilon_o - \alpha(z)\Delta T]$$

where $E(z)$ is the Young's modulus, $\nu(z)$ is the Poisson's ratio, $\alpha(z)$ is the thermal expansion coefficient and $\varepsilon_o$ denotes the strain at $z = 0$, which can be calculated from the equilibrium condition $\int_0^h \sigma(z)dz = 0$, where $h$ is the thickness of the sample. The resulting compressive thermal stress, calculated from the expression above, is in the order of MPa for the self-supporting film, and it is in the order of GPa for the film on Si substrate. It was shown not only in theoretical calculations [9,10,41], but also in experimental studies [42–45], that such a high hydrostatic pressure decreases the equilibrium vacancy concentration significantly. In this pressure range, the change can be as much as two orders of magnitude. As a result, the diffusion flux also decreases. The DLNT's on the other hand are support free, therefore there is no thermal stress contribution, which overall explains the relatively small growth rate in the planar sample.

We would like to emphasize that this is the first case that the influence of closed geometry and layer sequence on spinel growth between two oxide layers has been experimentally observed. The difference in the kinetics of the intermediate layer growth in a cylindrical and planar geometry has been compared and explained.

## Declaration of competing interest

The authors declare that they have no known competing financial interests or personal relationships that could have appeared to influence the work reported in this paper.

## Acknowledgements

Project no. TKP2021-NKTA-34 has been implemented with the support provided by the National Research, Development and Innovation Fund of Hungary, financed under the TKP2021-NKTA funding scheme. The work has been supported by the GINOP-2.3.2-15-2016-00041 project. The project is co-financed by the European Union and the European Regional Development Fund. This work was supported by the Development and Innovation Office NKFIH, Hungary, Grant No.: OTKA.K143724. The research reported in this paper and carried out at BME has been supported by the NRDI Fund TKP2021 BME-NVA based on the charter of bolster issued by the NRDI Office under the auspices of the Ministry for Innovation and Technology.

## References


[1] J. Philibert, Atom Movements, Diffusion and Mass Transport in Solids, Les Editions de Physique, Les Ulis, France, 1991.

[2] D. Beke, I. Szabó, Z. Erdélyi, G. Opposits, Diffusion-induced stresses and their relaxation, Mater. Sci. Eng. A 4 (2004) 387, http://dx.doi.org/10.1016/j.msea.2004.01.065.

[3] G. Schmitz, C. Ene, C. Nowak, Reactive diffusion in nanostructures of spherical symmetry, Acta Mater. 57 (2009) 2673, http://dx.doi.org/10.1016/j.actamat.2009.02.021.

[4] Y. Geguzin, Y. Klinchuk, I. Yu, L. Paritskaya, Peculiarities of voiding under interdiffusion in the samples with closed shape, Fiz. Met. Metalloved. 43 (1977) 602–609.

[5] Y. Geguzin, Diffusion Zone, Nauka, Moscow, 1979.

[6] V. Bogdanov, A. Gusak, L. Paritskaya, M. Yarmolenko, Characteristics of diffusion phase growth in cylindrical specimens, Metalophys. 12 (1990) 60–66.

[7] D. Beke, L. Kozéki, .I. Gődény, F. Kedves, Effect of stress and macroscopic deformation caused by interdiffusion on the growth of intermetallic layers, Def. Diff. Forum 66–69 (1989) 1357, http://dx.doi.org/10.4028/www.scientific.net/DDF.66-69.1357.

[8] L. Kozéky, D. Beke, Suppressed layer growth of intermetallic phases in cylindrical Cd-Ni diffusion couples, Def. Diff. Forum 95–98 (1993) 605, http://dx.doi.org/10.4028/www.scientific.net/DDF.95-98.605.

[9] Z. Erdelyi, G. Schmitz, Reactive diffusion and stresses in spherical geometry, Acta Mater. 60 (2012) 1807–1817, http://dx.doi.org/10.1016/j.actamat.2011.12.006.

[10] M. Roussel, Z. Erdelyi, G. Schmitz, Reactive diffusion and stresses in nanowires or nanorods, Acta Mater. 131 (2017) http://dx.doi.org/10.1016/j.actamat.2017.04.001.

[11] H. Fan, M. Knez, R. Scholz, D. Hesse, K. Nielsch, M. Zacharias, U. Gösele, Influence of surface diffusion on the formation of hollow nanostructures induced by the Kirkendall effect: The basic concept, Nano Lett. 7 (4) (2007) 993–997, http://dx.doi.org/10.1021/nl070026p.

[12] Q. Peng, X.-Y. Sun, J.C. Spagnola, C. Saquing, S.A. Khan, R.J. Spontak, G.N. Parsons, Bi-directional Kirkendall effect in coaxial microtube nanolaminate assemblies fabricated by atomic layer deposition, ACS Nano 3 (3) (2009) 546–554, http://dx.doi.org/10.1021/nn8006543.

[13] X. Chen, J. Li, Z. Sun, X. Fang, Z. Wei, F. Fang, X. Chu, S. Li, X. Wang, The formation and acceptor related emission behavior of ZnO/$ZnAl_2O_4$ core–shell structures, J. Alloys Compd. 571 (2013) 114–117, http://dx.doi.org/10.1016/j.jallcom.2013.03.198.

[14] E. Shkondin, H. Alimadadi, O. Takayama, F. Jensen, A. Lavrinenko, Fabrication of hollow coaxial $Al_2O_3$/$ZnAl_2O_4$ high aspect ratio freestanding nanotubes based on the Kirkendall effect, J. Vacuum Science & Technology A 38 (1) (2020) 013402, http://dx.doi.org/10.1116/1.5130176.

[15] Q. Zhao, Z. Yan, C. Chen, J. Chen, Spinels: Controlled preparation, oxygen reduction/evolution reaction application, and beyond, Chem. Rev. 117 (2017) 10121–10211, http://dx.doi.org/10.1021/acs.chemrev.7b00051.

[16] C. Zhang, J. Xiao, X. Lv, L. Qian, S. Yuan, S. Wang, P. Lei, Hierarchically porous $Co_3O_4$/C nanowire arrays derived from a metal-organic framework for high performance supercapacitors and the oxygen evolution reaction, J. Mater. Chem. A 4 (2016) 16516–16523, http://dx.doi.org/10.1039/C6TA06314D.

[17] X. Wu, K. Scott, $Cu_xCo_3 - xO_4$ ($0 \leq X \leq 1$) nanoparticles for oxygen evolution in high performance alkaline exchange membrane water electrolysers, J. Mater. Chem. 21 (2011) 12344–12351, http://dx.doi.org/10.1039/C1JM11312G.

[18] A. Indra, P. Menezes, N. Sahraie, A. Bergmann, C. Das, M. Tallarida, D. Schmeisser, P.S.M. Driess, Unification of catalytic water oxidation and oxygen reduction reactions: Amorphous beat crystalline cobalt iron oxides, J. Am. Chem. Soc. 136 (2014) 17530–17536, http://dx.doi.org/10.1021/ja509348t.

[19] M. Shevchenko, E. Jak, Integrated experimental phase equilibria study and thermodynamic modelling of the binary ZnO–Al2O3, ZnO–SiO2, Al2O3–SiO2 and ternary ZnO–Al2O3–SiO2 systems, Ceram. Int. 47 (15) (2021) 20974–20991, http://dx.doi.org/10.1016/j.ceramint.2021.04.098.

[20] Y. Okimura, H. Yokoi, K. Ohbayashi, K.-i. Shimizu, A. Satsuma, T. Hattori, Selective catalytic reduction of nitrogen oxides with hydrocarbons over Zn–Al–Ga complex oxides, Catal. Lett. 52 (1998) 157–161, http://dx.doi.org/10.1023/A:1019060512461.

[21] X. Li, Z. Zhu, Q. Zhao, L. Wang, Photocatalytic degradation of gaseous toluene over $ZnAl_2O_4$ prepared by different methods: A comparative study, J. Hard Mater. 186 (2011) 2089–2096, http://dx.doi.org/10.1016/j.jhazmat.2010.12.111.

[22] L. Cornu, M. Gaudon, V. Jubera, $ZnAl_2O_4$ as a potential sensor: Variation of luminescence with thermal history, J. Mater. Chem. C 1 (2013) http://dx.doi.org/10.1039/C3TC30964A.

[23] W.S. Tzing, W.-H. Tuan, The strength of duplex $Al_2O_3$-$ZnAl_2O_4$ composite, J. Mater. Sci. Lett. 15 (1996) 1395–1396.

[24] O. Kéri, E. Kocsis, Z.K. Nagy, B. Parditka, Z. Erdélyi, I.M. Szilágyi, Preparation of $Al_2O_3$ coated PVA and PVP nanofibers and $Al_2O_3$ nanotubes by electrospinning and atomic layer deposition, Revue Roumaine Chimie 63 (2018) 401–406, http://dx.doi.org/10.3390/molecules26195917.

[25] H. Zaka, S. Fouad, B. Parditka, A. Bekheet, H. Atyia, M. Medhat, Z. Erdélyi, Enhancement of dispersion optical parameters of $Al_2O_3$/ZnO thin films fabricated by ALD, Sol. Energy 205 (2020) 79–87, http://dx.doi.org/10.1016/j.solener.2020.05.025.

[26] M. Napari, J. Malm, R. Lehto, J. Julin, K. Arstila, T. Sajavaara, M. Lahtinen, Nucleation and growth of ZnO on PMMA by low-temperature atomic layer deposition, J. Vac. Sci. Technol. A 33 (1) (2015) 01A128, http://dx.doi.org/10.1116/1.4902326.

[27] G. Jáger, J. Tomán, L. Juhász, G. Vecsei, Z. Erdélyi, C. Cserháti, Nucleation and growth kinetics of $ZnAl_2O_4$ spinel in crystalline ZnO – amorphous $Al_2O_3$ bilayers prepared by atomic layer deposition, Scr. Mater. 219 (2022) 114857, http://dx.doi.org/10.1016/j.scriptamat.2022.114857.

[28] Y. Yin, C. Erdonmez, A. Cabot, A. Alivisatos, Colloidal synthesis of hollow cobalt sulfide nanocrystals, Ad. Func. Mater. 16 (2006) 1839, http://dx.doi.org/10.1002/adfm.200600256.

[29] G. Glodán, C. Cserháti, I. Beszeda, D. Beke, Production of hollow hemisphere shells by pure Kirkendall porosity formation in Au/Ag system, Appl. Phys. Lett. 97 (2010) 113109, http://dx.doi.org/10.1063/1.3490675.

[30] J. Svoboda, F. Fischer, Stress development during reaction of metallic nanospheres with gas, Acta Mater. 59 (2011) 61, http://dx.doi.org/10.1016/j.actamat.2010.09.001.

[31] G. Murch, A. Evteev, E. Levtheko, I. Belova, Basic principles of theory, experiment and application, Diffusion Fundam. 42 (2009) 1.

[32] H. Okada, Effect of physical nature of powders and firing atmosphere on $ZnAl_2O_4$ formation, J. Am. Ceram. Soc. 68 (1985) 58–63, http://dx.doi.org/10.1111/j.1151-2916.1985.tb15265.x.

[33] D. Branson, Kinetics and mechanism of the reaction between zinc oxide and aluminum oxide, J. Am. Chem. Soc. 48 (11) (1965) 591–595, http://dx.doi.org/10.1111/j.1151-2916.1965.tb14679.x.

[34] A. Gusak, Kinetics in Nanoscale Materials, John Wiley & Sons, Ltd, 2014, pp. 67–98.

[35] A. Gusak, N. Storozhuk, Competition of k and f sinks during void formation, Phys. Metals Metallogr. 114 (2013) 197, http://dx.doi.org/10.1134/S0031918X13030071.

[36] T. Zaporozhets, N. Storozhuk, A. Gusak, Competition of voiding and Kirkendall shift during compound growth in reactive diffusion–alternative models, Metallofiz. Noveishie Tekhnol. 38 (10) (2016) 1279—1292, http://dx.doi.org/10.15407/mfint.38.10.1279.

[37] O. Louchev, Y. Sato, Influence of nanoscale substrate curvature on growth kinetics and morphology of surface nuclei, J. Appl. Phys. 84 (12) (1998) 6673–6679, http://dx.doi.org/10.1063/1.369043.

[38] A. Gusak, Flux-driven lateral grain growth during reactive diffusion, Metallofiz. Noveish. Tekhnol. 42 (10) (2020) 1335–1346, http://dx.doi.org/10.15407/mfint.42.10.1335.

[39] Z. Erdélyi, D. Beke, Stress effects on diffusional interface sharpening in ideal binary alloys, PhysRevB 68 (2003) 092102, http://dx.doi.org/10.1103/PhysRevB.68.092102.

[40] A. Giannakopoulos, S. Suresh, M. Finot, M. Olsson, Elastoplastic analysis of thermal cycling: Layered materials with compositional gradients, Acta Metall., Mater. 43 (4) (1995) 1335–1354, http://dx.doi.org/10.1016/0956-7151(94)00360-T.

[41] D. Connétable, P. Maugis, Effect of stress on vacancy formation and diffusion in fcc systems: Comparison between DFT calculations and elasticity theory, Acta Mater. 200 (2020) 869–882, http://dx.doi.org/10.1016/j.actamat.2020.09.053.

[42] F. Kedves, G. Erdélyi, Diffusion under high pressure, Defect Diffusion Forum 66–69 (1991) 175–188, http://dx.doi.org/10.4028/www.scientific.net/DDF.66-69.175.

[43] H. Mehrer, The Effect of Pressure on Diffusion, Defect Diffusion Forum 129–130 (1996) 57–76, http://dx.doi.org/10.4028/www.scientific.net/DDF.129-130.57.

[44] R.M. Emrick, Effect of Pressure on Vacancy Concentrations in Platinum, Phys. Rev. B 6 (4) (1972) 1144–1148, http://dx.doi.org/10.1103/PhysRevB.6.1144, Publisher: American Physical Society.

[45] R.P. Huebener, C.G. Homan, Pressure Effect on Vacancy Formation in Gold, Phys. Rev. 129 (3) (1963) 1162–1168, http://dx.doi.org/10.1103/PhysRev.129.1162.